Methods in Oceanography 17 (2016) 232–250

Contents lists available at ScienceDirect

Methods in Oceanography

journal homepage: www.elsevier.com/locate/mio

Full length article

A topological approach for quantitative comparisons of ocean model fields to satellite ocean color data

Hannah R. Hiester [a,*], Steven L. Morey [a], Dmitry S. Dukhovskoy [a], Eric P. Chassignet [a], Vassiliki H. Kourafalou [b], Chuanmin Hu [c]

[a] Center for Ocean-Atmospheric Prediction Studies, Florida State University, 2000 Levy Avenue, Building A, Suite 292, Tallahassee, FL 32306-2741, USA

[b] Rosenstiel School of Marine and Atmospheric Sciences, University of Miami 4600 Rickenbacker Causeway, Miami, FL 33149-1098, USA

[c] Optical Oceanography Laboratory, College of Marine Science, University of South Florida, 140 7th Avenue S, MSL119, St. Petersburg, FL 33701, USA

HIGHLIGHTS

- A topological metric is introduced for comparing differing but related geophysical fields.
- The metric is demonstrated by comparing satellite ocean color data to model salinity.
- The metric allows quantitative comparison of spatial characteristics of observed and modeled fields.

ARTICLE INFO

Article history:
Received 5 April 2016
Received in revised form
6 September 2016
Accepted 12 September 2016
Available online 14 November 2016

Keywords:
Satellite data
Ocean model
Ocean color
Sea surface salinity

ABSTRACT

In an effort to more fully employ underutilized satellite observations in ocean modeling, this work demonstrates a method for quantifying the agreement between time-evolving spatial features evident in fields of differing, but functionally related, variables that are more commonly compared qualitatively via visual inspection. This is achieved through application of the Modified Hausdorff Distance metric to the evaluation of ocean model simulations of surface salinity near riverine sources using satellite ocean color data. The Modified Hausdorff Distance is a metric from the field of topology designed to compare shapes and the methodology provides quantitative assessment of similarity of spatial fields. The Mod-

* Corresponding author.
E-mail address: hhiester@fsu.edu (H.R. Hiester).

http://dx.doi.org/10.1016/j.mio.2016.09.005

Shape comparison
Hausdorff distance

ified Hausdorff Distance can be applied for comparison of many geophysical and ecological fields that vary spatially and temporally. Here, the utility of the metric is demonstrated by applying it to evaluate numerical simulations of the time-evolving spatial structure of the surface salinity fields from three ocean models in the vicinity of large riverine sources in the northeast Gulf of Mexico. Using the Modified Hausdorff Distance, quantitative comparison of modeled sea surface salinity contours to contours of a gridded satellite-derived ocean color product is made under the assumption that the modeled fields are related to optically significant quantities that indicate the spatial extent of riverine influenced water. Three different ocean models are evaluated and are compared individually to the satellite data. The sea surface salinity values and ocean color index values that most closely match (lowest Modified Hausdorff Distance score) are identified for each model. The Modified Hausdorff Distance scores for these best pairings are used to both determine the degree to which surface salinity fields from the models match the satellite observations and obtain an empirical relationship between the two variables for each model. Furthermore, the best pairings are compared between models allowing key differences in the simulated riverine water distributions to be distinguished. The Modified Hausdorff Distance proves a robust and useful diagnostic tool that has the potential to be utilized in many geophysical applications and facilitates the use of satellite ocean color data for quantitative evaluation of hydrodynamic ocean models.

1. Introduction

For decades satellite sensors have been used to detect the color of the ocean surface by measuring light reflectance in different spectral bands (McClain, 2009). These ocean color data products have been utilized to identify and analyze ocean features that affect pigment and particulate content of the water and hence the ocean color, including oil spills, algal blooms and river plumes (e.g. Hu et al., 2004; Androulidakis and Kourafalou, 2013; Liu et al., 2013; Hu et al., 2015). They have also been integrated into observation and detection systems for harmful algal blooms and oil spills (e.g. Stumpf et al., 2003; Brekke and Solberg, 2005; Hu et al., 2016). With both broad spatial and frequent temporal coverage, satellite ocean color observations also have the potential to be valuable resources for numerical ocean modeling, however the ocean circulation modeling community has not fully capitalized on the utility of this data.

Satellite ocean color data have been used for ocean model assessment qualitatively, as patterns evident in the ocean color are often similar to, and may generally be visually compared to, features in dynamical fields (e.g. Binding and Bowers, 2003; Gregg et al., 2003; Chassignet et al., 2006; Liu et al., 2011; Schiller et al., 2011). Quantitative comparisons generally rely on point-wise differences that demand the same field be used and/or an empirical relationship between different but related fields is determined (e.g. Binding and Bowers, 2003; Gregg et al., 2003; Gregg, 2008; Mariano et al., 2011; Chaichitehrani et al., 2014; Zhang et al., 2014). While the types of statistical measures derived from point-wise comparisons (e.g. biases or correlations) are useful, they do not necessarily provide comparison of spatial distributions and/or shape that are related to circulation patterns or dynamical processes, and neither are they expressly designed for such a purpose. In an effort to more fully utilize the vast amount of remotely sensed data for ocean model assessment and analysis, the objective of this work is to apply and demonstrate the potential of a metric called the Modified Hausdorff Distance (MHD) to quantitatively compare spatial and temporal patterns derived from satellite ocean color

observations to ocean circulation models. It is anticipated that the methodology introduced here will have extensions in future to new satellite observations (such as surface salinity) and the development of cost functions for adjoint data assimilation techniques.

2. Background

The MHD originates from the field of topology and is designed specifically to compare shapes (Dubuisson and Jain, 1994). The MHD and Hausdorff distance, from which the former is derived, are frequently used in imaging software for object location and pattern recognition (Huttenlocher et al., 1993; Huttenlocher and Rucklidge, 1993; Rucklidge, 1997; Daoudi et al., 1999; Zhang and Lu, 2004). There has been some application to analysis of geospatial data, an example being precipitation patterns where the Hausdorff distance forms one component of a Forecast Quality Index (e.g. Venugopal et al., 2005; Nan et al., 2010) and application of the MHD for skill assessment of sea ice models based on analysis of spatial distribution of sea ice concentration (Dukhovskoy et al., 2015). However, the metric has not been widely utilized in oceanographic applications. The particular application considered here compares ocean model surface salinity fields with satellite ocean color data near a large river source, the Mississippi River. This presents the opportunity to utilize ocean color data from satellites for quantitative model assessment and intermodel comparison in a region with high spatial and temporal variability of the salinity field.

The Mississippi River enters the northeast Gulf of Mexico (NEGoM) through several channels along the end of the Mississippi Delta. This study focuses on the area east of the Mississippi Delta where the shelf is nearly non-existent and small mesoscale deep ocean eddies dominate the circulation field over the nearby DeSoto Canyon. The domain for this analysis extends from approximately 50 km west of the Mississippi Delta eastward to Apalachicola Bay in North Florida, and from 28° N northward to the coast (Fig. 1). The surface salinity in this region is influenced by several rivers and is dominated by outflow from the Mississippi River (Fig. 2). During the fall and winter months, the Mississippi River plume tends to be trapped closely to the coast westward of the study domain (Morey et al., 2003a, 2005). In the spring and summer, reversal of the climatological wind allows the plume to spread eastward over the DeSoto Canyon region (Morey et al., 2003b; Walker et al., 2005) (Fig. 3). Interaction with circulation features such as the Loop Current and Loop Current Eddies leads to a complex structure, with salinity contours forming intricate shapes with filaments extending across the domain (Figs. 3 and 4, Walker et al., 1996; Morey et al., 2003b; Schiller et al., 2011; Androulidakis and Kourafalou, 2013). The geometry of these fields presents a challenging system for the MHD to assess, making the region and the system analyzed an excellent scenario for demonstration and evaluation of the utility of the metric.

3. Data and methods

This study demonstrates application of the MHD for comparing satellite-derived and ocean model fields of different, but related quantities. In particular, an ocean color product derived from satellite optical data is compared to salinity fields from three different models to evaluate the models' representations of the distribution of riverine water. In this section, the MHD and Hausdorff distance (from which the MHD is derived) are introduced, the ocean color product and the model simulations are described, and the application of the MHD and diagnostic techniques are detailed.

3.1. The Modified Hausdorff Distance

The Hausdorff Distance, from which the Modified Hausdorff Distance is derived, is a topological metric commonly used in the context of visual imaging for pattern recognition and shape matching, with utility for applications such as facial recognition (Huttenlocher and Rucklidge, 1993; Huttenlocher et al., 1993; Rucklidge, 1997; Daoudi et al., 1999; Zhang and Lu, 2004). The Hausdorff Distance is very sensitive to outliers within a dataset and modified versions (the Modified Hausdorff Distance, MHD) of the metric that have a more robust response to both outliers and noise have been

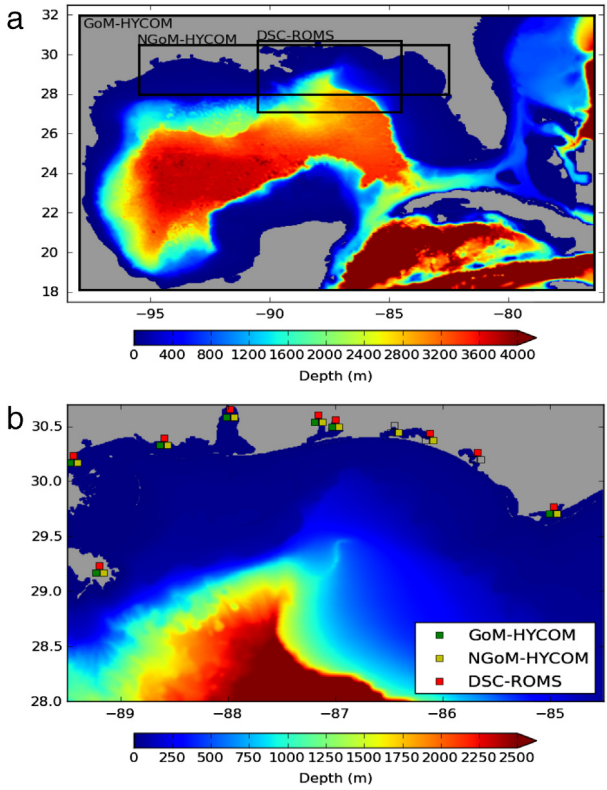

Fig. 1. (a) Model domain and bathymetry for the GoM-HYCOM simulation. Boxes represent domains for the DSC-ROMS and NGoM-HYCOM (model configurations and acronyms are defined in Section 3.3). (b) Subdomain common to all models used for analysis. The bathymetry is shown for the DSC-ROMS configuration. The squares indicate which river sources are simulated in each model (determined by the presence or absence of fill color). (For interpretation of the references to color in this figure legend, the reader is referred to the web version of this article.)

investigated (Dubuisson and Jain, 1994; Mattern et al., 2010). Here, following Dubuisson and Jain (1994) and Dukhovskoy et al. (2015), the version of the MHD used is given by

$$\mathrm{MHD} = \max\left\{d\left(A,B\right), d(B,A)\right\}, \tag{1}$$

where

$$d\left(A,B\right) = \frac{1}{|A|}\sum_{a\in A} d(a,B); \quad d\left(a,B\right) = inf_{b\in B} d\left(a,b\right), \tag{2}$$

and

$$d\left(B,A\right) = \frac{1}{|B|}\sum_{b\in B} d(A,b); \quad d\left(A,b\right) = inf_{a\in A} d\left(a,b\right) \tag{3}$$

with A the set of points on one contour, B the set of points on a second contour and $d(a, b)$ the distance between those points (here, great circle distance, km). In simple terms, it may be considered to be the largest of the average of the minimum distances between each point on contour A and contour B and the average of the minimum distances between each point on contour B and contour A. A schematic illustrating application of the methodology given in (1)–(3) for computing the MHD can be found in Dukhovskoy et al. (2015, their Figure 3 and related text).

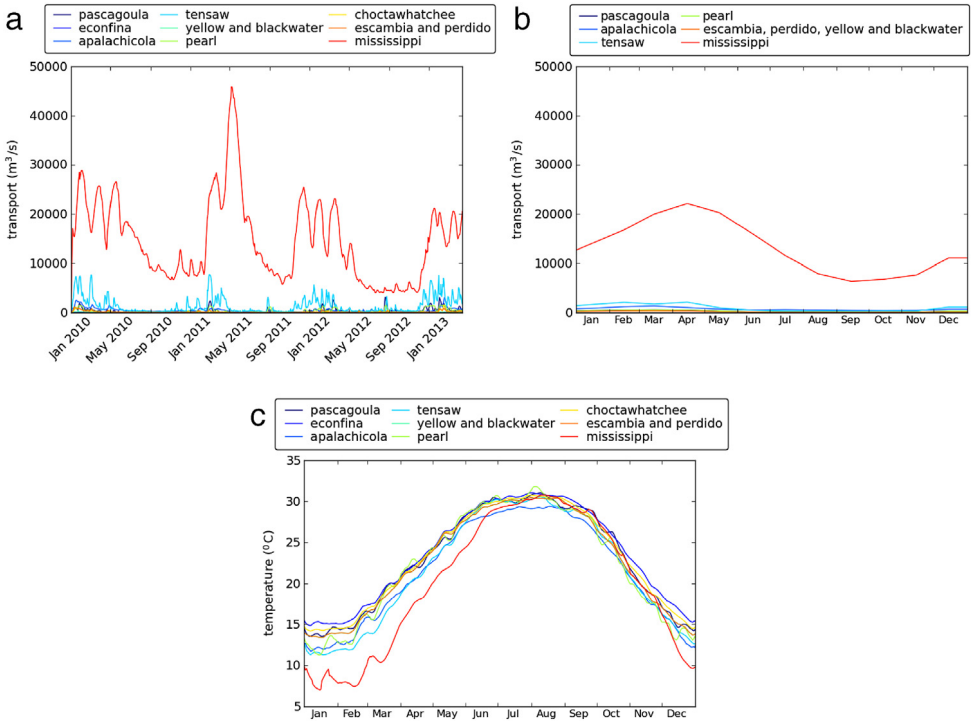

Fig. 2. (a) Daily river discharge calculated from US Geological Survey data used for DSC-ROMS transport. NGoM-HYCOM uses the same data source to calculate daily river transport and has similar variation and magnitude. (b) Monthly climatology used for GoM-HYCOM river transport. (c) Temperature climatology calculated from NOAA tides and currents data used for DSC-ROMS. For river locations see Fig. 1.

The MHD increases as the shapes of the contours become increasingly different and decreases as they become more similar. It is noted that the MHD is a topological distance and $d(a, b)$ in Eqs. (2) and (3) has units of distance (kilometers in the examples shown here). However, in general, the value of the MHD should be viewed simply as a score with a lower value indicating a better match, and is therefore shown without units here. An example illustrating this metric for comparing different Sea Surface Salinity (SSS) contours from a model is shown in Fig. 5. In this example, the SSS = 33 contour from one of the models used in this study (the DeSoto Canyon simulation based on the Regional Ocean Modeling System, DSC-ROMS, described in Section 3.3) at a particular "control" time ($t = T$) is compared to SSS = 33 contours from the simulation at times $T + \delta t$ for $\delta t \in [-93, -69, -45, -21, 3, 27, 51, 75, 99]$ hours. As expected, the SSS contour shapes most closely match for the shortest time offset of 3 hours, and become increasingly different as the magnitude of the time offset increases. The MHD values computed between the "control" contour and the contours at other times mirror these changes, decreasing and increasing as the contour shapes become more and less similar, respectively. Hence, the metric can be used to provide a measure of the agreement between the contour shapes.

Unlike other shape comparison metrics such as Root Mean Square Deviation and Mean Dispersion, Dukhovskoy et al. (2015) show an increase in MHD score when a shape is compared to rotations and translations of itself. This is desirable for the river plume comparison considered here, as orientation and location of certain features (e.g., filaments) in surface salinity contours are important characteristics and manifest as differences in rotation (orientation) and translation (location) of contours. Dukhovskoy et al. (2015) also show that the MHD is robust to noise, with contours being shown to be similar (small MHD score) if the amplitude of the noise is small but also showing an increase in the MHD score (i.e. a difference in the contours) as the amplitude of the noise grows larger.

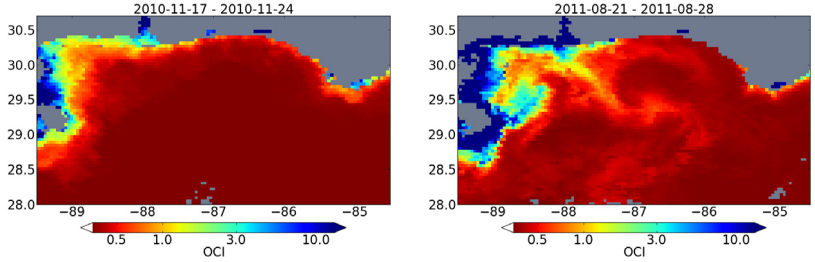

(a) Winter satellite.

(b) Summer satellite.

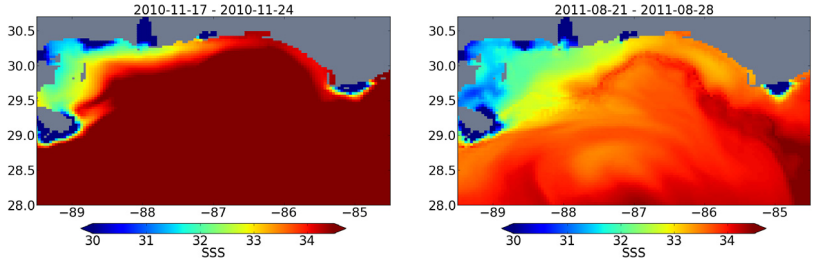

(c) Winter GoM-HYCOM.

(d) Summer GoM-HYCOM.

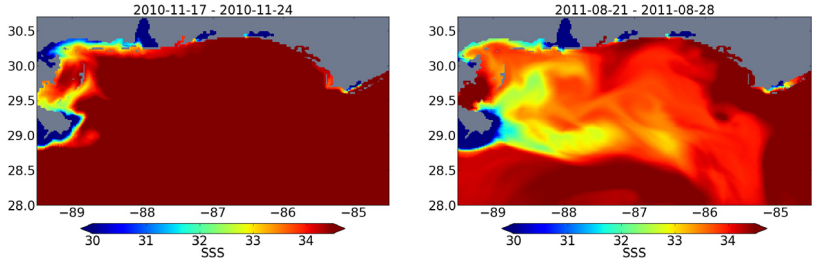

(e) Winter NGoM-HYCOM.

(f) Summer NGoM-HYCOM.

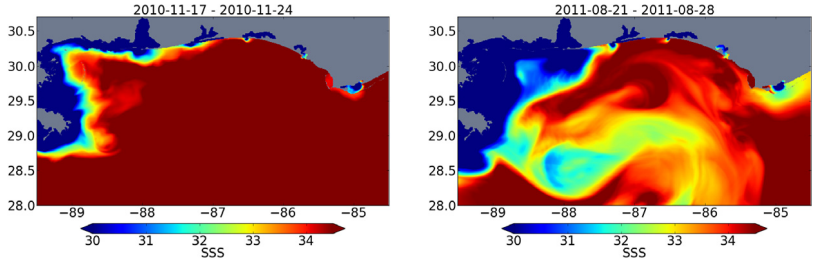

(g) Winter DSC-ROMS.

(h) Summer DSC-ROMS.

Fig. 3. Example 8-day averaged fields of typical winter (left) and summer (right) Ocean Color Index (OCI, a–b) and Sea Surface Salinity (SSS) fields from GoM-HYCOM (c–d), NGoM-HYCOM (e–f) and DSC-ROMS (g–h). Animations for the entire time periods from each of the above can be found at: https://youtu.be/w3mf0EtYWOU (satellite), https://youtu.be/OogU7VVn4fI (GoM-HYCOM), https://youtu.be/2HdHTF7CCAg (NGoM-HYCOM) and https://youtu.be/YyQmd4OxzB0 (DSC-ROMS).

Robustness to noise is a very useful property for comparing river plumes. If small-scale features (small-amplitude noise) are diffused and therefore smoothed out of the contours of one model relative to the contours of another slightly less diffuse model, then ideally a metric will still be able to determine

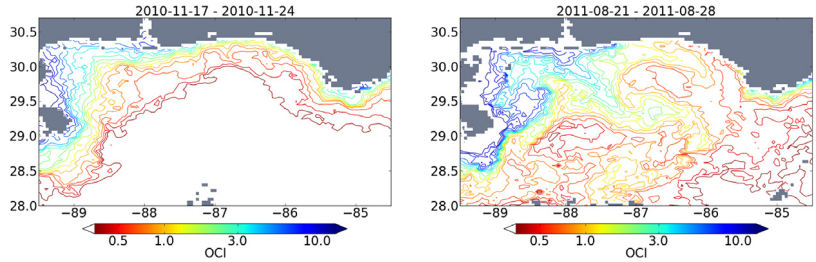

(a) Winter satellite. (b) Summer satellite.

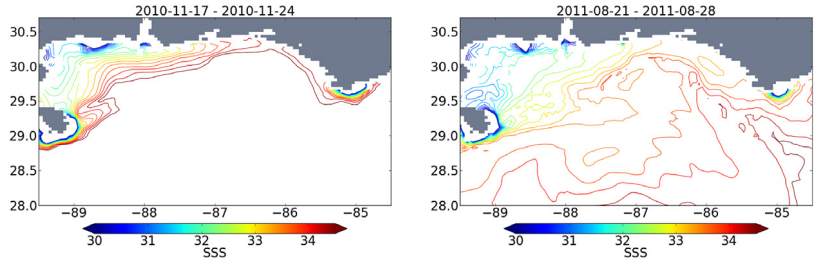

(c) Winter GoM-HYCOM. (d) Summer GoM-HYCOM.

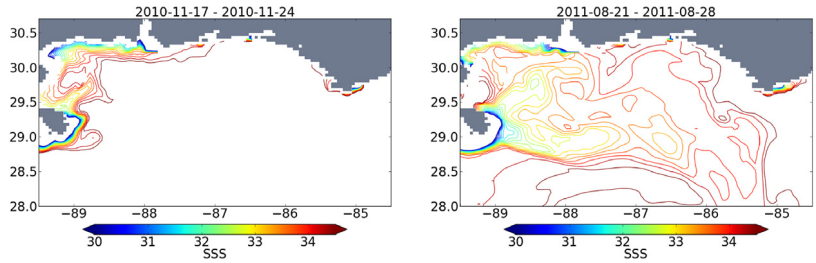

(e) Winter NGoM-HYCOM. (f) Summer NGoM-HYCOM.

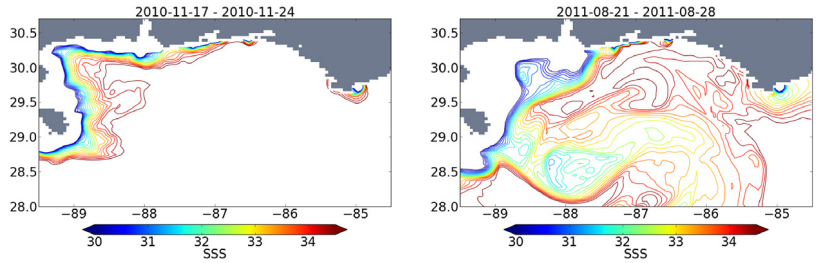

(g) Winter DSC-ROMS. (h) Summer DSC-ROMS.

Fig. 4. Examples of contours of the fields shown in Fig. 3. The ocean model data have been regridded to the 4-km grid of the OCI product. Animations for each of the above can be found at: https://youtu.be/AEdhNoDk_P8 (satellite), https://youtu.be/5tn7b2PIjuQ (GoM-HYCOM), https://youtu.be/eg4IJoDZvK0 (NGoM-HYCOM) and https://youtu.be/xvmjccO5JiA (DSC-ROMS).

whether there is a general similarity in shape between the two sets of contours. At the same time, if one model is notably more diffusive than another such that the plume shape and hence contours are warped significantly in the diffuse case relative to the less diffusive case (i.e. large-amplitude noise in

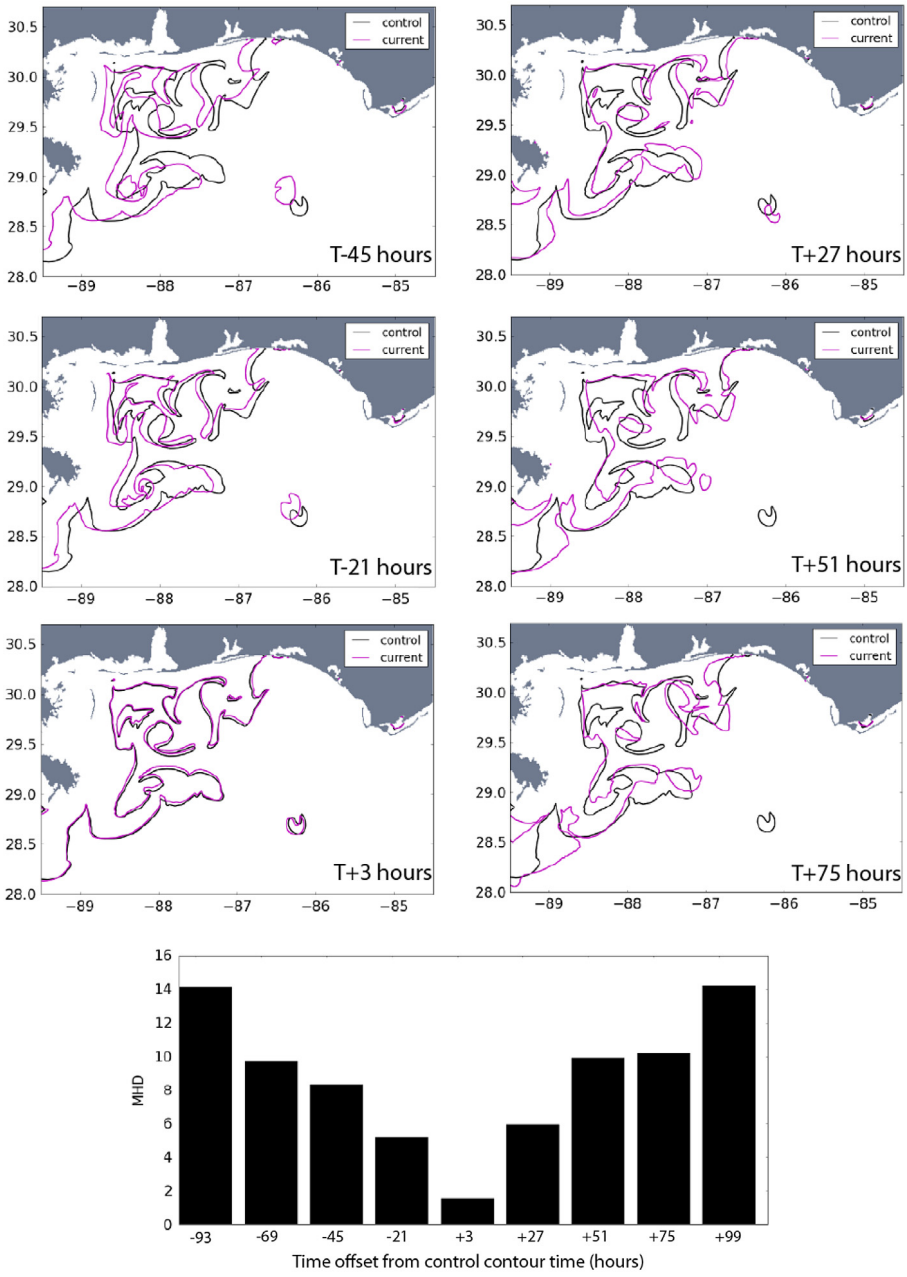

Fig. 5. Maps of contours of SSS = 33 from the DSC-ROMS simulation. On each plot, the black contour is from model time T, and the magenta contours are from the model time indicated on each plot. Bottom: MHD values showing the agreement of SSS = 33 contours from the model control time (T) and nine different model times. (For interpretation of the references to color in this figure legend, the reader is referred to the web version of this article.)

the diffuse case), the metric should be able to determine that there is a lack of similarity between the two and return a larger MHD score.

3.2. Satellite Ocean Color Index

An Ocean Color Index (OCI, Hu et al., 2012) derived from data from the Moderate Resolution Imaging Spectroradiometer (MODIS) is used as a proxy for identifying riverine influenced water to evaluate the ocean model salinity fields in the vicinity of the Mississippi River. The algorithm is based on a three-band subtraction for relatively clear waters (chlorophyll a concentration <0.25 mg m^{-3}), but switches to a blue/green band ratio algorithm for more productive waters. MODIS data (NASA reprocessing # 2014.0, processed using SeaDAS version 7.2) were obtained from the NASA Goddard Space Flight Center (GSFC, http://oceancolor.gsfc.nasa.gov) and processed with the most current algorithms. This OCI product has 4 km resolution and is temporally averaged over eight days.

The choice of OCI presents a compromise between accuracy, data availability, and applicability in tracking riverine waters. In addition to fresh water, rivers discharge suspended sediment, Colored Dissolved Organic Matter (CDOM), and nutrients that facilitate primary productivity (chlorophyll-rich phytoplankton growth). Relationships between CDOM and SSS have been previously used to investigate oceanographic and estuarine waters (e.g. Hu et al., 2003; Green and Sosik, 2004; Chaichitehrani et al., 2014; Chonga et al., 2014). Therefore, CDOM from MODIS measurements might be considered an obvious candidate to use as proxy for SSS to trace plume waters. However, from the perspective of algorithms, it is difficult to derive an accurate CDOM product in riverine waters for a number of reasons including uncertainties in atmospheric correction in the blue bands and difficulty in separating CDOM and phytoplankton in CDOM-rich waters.

As an alternative to a satellite CDOM product, the OCI is derived from an empirical algorithm that accounts for both phytoplankton and CDOM thus making it a good proxy for representation of total absorption (Hu et al., 2012), similar to the use of the light attenuation (Kd derived from the blue–green band ratio algorithm, which is essentially a total absorption as well) to trace the Amazon River plume (Del Vecchio and Subramaniam, 2004). As a river plume advects offshore and mixes with ambient seawater, most sediment particles settle to the bottom in near shore waters while CDOM and often phytoplankton decrease, resulting in a decrease in OCI. Hence, a higher OCI tends to correspond to fresher water closer to the river mouth (i.e. a lower SSS value) than further offshore and vice versa. Because OCI contains information about both CDOM and phytoplankton in offshore waters where suspended sediments are low, it is therefore reasonable to assume that there is a correspondence between OCI and SSS, particularly in the CDOM rich riverine waters. One exception to this is in coastal upwelling zones where phytoplankton are abundant but CDOM may be low, leading to a false interpretation of the OCI–SSS relationship. However, in the study region, intense coastal upwellings are rare (e.g., Muller-Karger et al., 2015), making OCI a reasonable proxy to trace plume waters. In addition, the availability of OCI data makes it a useful product. Since 2015, NASA has made OCI the standard (default) chlorophyll data product, where 4-km resolution global data are generated and provided to the community at daily, 8-day, and monthly intervals. Note that OCI is used here as a relative index to trace plume waters rather than as an index to derive absolute SSS values.

3.3. Numerical models

Three ocean model simulations are evaluated, two of which use the Hybrid Coordinate Ocean Model (HYCOM) and one of which uses the Regional Ocean Modeling System (ROMS). They differ in numerical methods and configuration. Of particular relevance are differences in: data assimilation (assimilative or not), as this impacts representation of the mesoscale features that have been shown to impact riverine water spreading in the NEGoM (e.g. Morey et al., 2003b; Schiller et al., 2011); horizontal spatial resolution, which can impact both representation of fields and horizontal mixing; surface forcing, particularly as the wind patterns have been shown to impact riverine water distribution in the NEGoM (e.g. Morey et al., 2003a,b); and parameterization of river inflow. This information is summarized in Table 1. For further information, the reader is directed to the cited references and references therein.

Table 1
Summary of the three model simulations.

Simulation	GoM-HYCOM	NGoM-HYCOM	DSC-ROMS
Data-assimilation	Data-assimilative	Free-running	Free-running
Horizontal resolution	1/25°	1/50°	1 km
River parameterization	Surface freshwater flux with enhanced vertical diffusivity	Surface freshwater flux with enhanced vertical diffusivity and barotropic adjustment	Temperature, salinity and momentum point source (or series of point sources).
Surface forcing	NOGAPS	COAMPS	CFSR

3.3.1. The Gulf of Mexico Hybrid Coordinate Ocean Model

The Hybrid Coordinate Ocean Model (HYCOM) is a finite-difference primitive equation hydrostatic ocean circulation model (Bleck, 2002; Chassignet et al., 2003, 2006). It incorporates a flexible vertical coordinate system allowing smooth transition between isopycnal, terrain-following (sigma) and pressure coordinates to meet the demands of different ocean modeling challenges, for example complex bathymetry or changing stratification. HYCOM is used operationally by the US Navy and National Ocean Atmospheric and Administration (NOAA) in the global ocean forecasting systems (Chassignet et al., 2005; Metzger et al., 2014). In this paper, a data-assimilative HYCOM Gulf of Mexico hindcast product is evaluated and will be referred to as GoM-HYCOM. The archived data were obtained from the HYCOM server (HYCOM-31.0, http://hycom.org/data/goml0pt04/expt-31pt0). The domain encompasses the full Gulf of Mexico, [−98.0° W, −76.4° W] and [18.90° N, 31.96° N] in longitude and latitude respectively (Fig. 1). The horizontal resolution is (1/25)° of longitude by (cos(latitude)/25)° in latitude resulting in grid spacing of approximately 3.8–4.2 km. The vertical grid has twenty layers, which are primarily isopycnal-following in the stratified deep ocean, transitioning to pressure levels in the mixed layer and terrain-following (sigma) coordinates in shallow water. The model is forced at the lateral open boundaries with climatology fields derived from a 1/12° HYCOM model simulation of the Atlantic Ocean (Kourafalou et al., 2009). The surface forcing is provided by the Navy Operational Global Atmospheric Prediction System (NOGAPS, Rosmond et al., 2002). Data-assimilation is incorporated using the Navy Coupled Ocean Data Assimilation (Cummings, 2005). River runoff is specified at 40 locations along the coast using a monthly climatology. The river input is implemented as a virtual salt flux at the surface (Huang, 1993; Schiller and Kourafalou, 2010). The virtual salt flux, S_f, is calculated from precipitation (P), evaporation (E) and river input (R), with $S_f = [-(P - E) - R]S/\alpha_0$ where S is the salinity in the top layer of the model and α_0 is a reference specific volume. S_f is then used to calculate the salinity increment in the top layer of the model, $dS = S_f dt_{bclin} g/dp$ where dt_{bclin} is the baroclinic time step, g is gravity and dp is the layer thickness in pressure units. At each baroclinic time step, the salinity in the top layer of the model, S, is updated to account for changes due to freshening via the virtual salt flux as $S(t + dt_{bclin}) = S(t) + dS$ where t is time. For each river, the freshwater flux is distributed over several ocean grid points adjacent to the river source and an enhanced diffusivity is employed over a depth of 6 m to mix the source water through the water column. The surface salinity is relaxed to climatology.

3.3.2. The northern Gulf of Mexico Hybrid Coordinate Ocean Model

A northern Gulf of Mexico free-running (non-assimilative) configuration of HYCOM (NGoM-HYCOM) has been developed (Schiller et al., 2011; Androulidakis and Kourafalou, 2013; Kourafalou and Androulidakis, 2013) with an advanced river input representation that extends the standard HYCOM code (Section 3.3.1) to include momentum fluxes (in addition to salt fluxes) at the river mouth and the ability to distribute the river input both vertically at the river mouth and across estuarine cells (Schiller and Kourafalou, 2010). The domain extends across the Louisiana–Texas shelf and the Mississippi–Alabama–Florida shelf [−95.52° W, −82.52° W] and [27.98° N, 30.70° N] in longitude and latitude respectively (Fig. 1) and has 1/50° horizontal resolution. This simulation has thirty vertical layers, 15 of which are at fixed depths in the upper 40 m of the water column (transitioning to terrain-following in shallow water). The model is nested in the 1/25° data-assimilative Gulf of Mexico HYCOM model (Section 3.3.1) and atmospheric forcing is derived from the

Coupled Ocean/Atmospheric Mesoscale Prediction System (COAMPS, Hodur et al., 2002). Daily average freshwater discharges derived from United Stated Geological Survey data are prescribed for 16 rivers, with monthly climatologies imposed for the Pearl River and Mobile Bay. These rivers are specified as point sources (or multiple point sources for the Mississippi River) and there is no relaxation to climatology. In addition, the barotropic pressure change of the water column is adjusted to take into consideration the additional pressure exerted by the additional mass, and hence volume, of the river inflow.

3.3.3. The Regional Ocean Modeling System northeast Gulf of Mexico configuration

The Regional Ocean Modeling System (ROMS) is a finite-difference primitive equation ocean circulation model that employs the hydrostatic and Boussinesq approximations (Shchepetkin and McWilliams, 2003, 2005). ROMS uses a variation of sigma coordinates (sometimes referred to as *s*-coordinates) in the vertical that can be stretched to allow increased resolution in areas of interest (Song and Haidvogel, 1994).

The domain for the ROMS configuration encompasses the De Soto Canyon region in the northeast Gulf of Mexico (Fig. 1) and will be referred to as DSC-ROMS (https://data.gulfresearchinitiative.org/data/R1.x138.080:0022/). The domain extends from the Mississippi Delta to Apalachicola Bay [−90.5° W, −84.5° W] and [27.1° N, −30.7° N] in longitude and latitude respectively. The model grid has one kilometer horizontal grid spacing with 40 layers in the vertical dimension, compressed to increase resolution in the upper part of the water column. The model is nested in the 1/12° data-assimilative global HYCOM model and atmospheric forcing is derived from the Climate Forecast Reanalysis System (CFSR, Saha et al., 2010). The river input is treated as vertically distributed source terms for temperature, salinity, and momentum. Daily average discharges are calculated from US Geological Survey data while temperature climatology is calculated from NOAA tides and currents buoy data (Fig. 2).

3.4. Diagnostics

3.4.1. Procedure overview

Two-dimensional contours (isolines) of select values are computed from the satellite OCI fields and from the SSS fields for each of the ocean models. The OCI generally decreases with distance from the river sources as the riverine waters spread and mix with seawater. Conversely, the SSS values generally increase with distance from the river sources as the fresh river water mixes with the saline ambient water. These fields are thus indicators of the region influenced by riverine water, and the similarity of their spatial patterns is quantified using the MHD metric. Conducting this analysis on multiple pairings of values of SSS and OCI contours identifies the SSS–OCI relationships for each model and the differences in these pairings are utilized to compare the river plume representations between models.

3.4.2. Preprocessing

The satellite product and model data have differing time resolution, spatial resolution, and spatial domain bounds. To compare these datasets, the coarsest common temporal and spatial resolutions are adopted and the smallest common spatial domain is used (Fig. 1). (When determining common spatial domains, regions of the nested NGoM-HYCOM and DSC-ROMS in which relaxation to the parent model fields takes place are not considered as part of the model domains for analysis purposes.) The satellite OCI dataset used in this study has the coarsest temporal resolution of the datasets with an eight-day average, as well as the coarsest spatial resolution with 4 km grid spacing. Therefore, the model data are temporally averaged over eight days and regridded to the satellite product's 4 km grid using a nearest neighbor average. The land and cloud masks from the satellite data are then applied such that only areas with data present in all products are compared at each time. The smallest common spatial domain is determined by the DSC-ROMS model for the eastern and western boundaries and the NGoM-HYCOM for the southern boundary. The northern boundary is bounded by the Mississippi–Alabama–Florida coastline. The resultant domain bounds used are

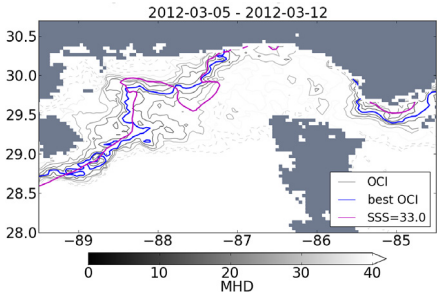

Fig. 6. Ocean Color Index (OCI) contours (gray and blue) and the SSS = 33 contour (magenta) from the 8-day averaged DSC-ROMS salinity field. The OCI contours are shaded based on the MHD computed between them and the SSS = 33 contour. The OCI = 1.65 contour has the lowest MHD (12.20) and is in blue. Dashed contours represent OCI contours with MHD greater than 40. (For interpretation of the references to color in this figure legend, the reader is referred to the web version of this article.)

therefore [−89.5° W, −84.5° W] and [28.0° N, 30.7° N] in longitude and latitude respectively, and only contours within this region are compared.

3.4.3. Application of the Modified Hausdorff Distance

The similarity between contours of OCI from the satellite data and contours of SSS from each of the models is quantified by calculating the MHD. An example illustrating application of the MHD to compare SSS and OCI contours is shown in Fig. 6. In this example, the SSS = 33 contour from a particular 8-day average salinity field from the DSC-ROMS simulation processed as described in Section 3.4.2 is shown by the magenta line. Contours for several satellite OCI values are overlain in gray, with the shading of those contours indicating the MHD computed between them and the model SSS = 33 contour. (OCI contours that correspond to an MHD > 40 are dashed.) The OCI contour (OCI = 1.65) that most closely matches the model SSS = 33 contour determined by the lowest (best) MHD score (12.20) is shown by the blue line.

A further example of a satellite OCI field and a model SSS field and corresponding MHD values for all tested pairs of SSS–OCI contours at a particular time is shown in Fig. 7. A smaller MHD indicates a better correspondence between the SSS and OCI contours. As the SSS increases, the value of the OCI with the smallest MHD increases reflecting the inverse relationship between SSS and OCI and suggestive of an OCI–SSS functional relationship (Fig. 7(c)). In this example, fresher (higher OCI) contours are found closer to the coastline where they are similar in shape leading to smaller MHD values. Further from the shore, the higher salinity (lower OCI) contours have more complex shapes that are less similar and the MHD values for OCI–SSS pairings that most closely match reflect this lack of similarity by increasing correspondingly. It is noted that in the case of cloud cover, contours may become segmented. Since the contours are decomposed into a set of discrete points for the MHD calculation this segmentation does not affect the calculation of the MHD.

While both SSS and OCI are good indicators of riverine-influenced water, the functional relationship between SSS and OCI values is not known. To determine this relationship empirically for the SSS field for each model, the MHD is calculated for all pairs of OCI–SSS contour values, as shown by the example in Fig. 7. The MHD values are then averaged over time for each OCI–SSS pairing. The best pairings (lowest MHD) over all times are then identified and a polynomial is fit to these data. This yields an empirical functional relationship between SSS and OCI for each model. Inspection of the MHD for these optimum OCI–SSS pairings also provides information about the model agreement with the satellite data.

4. Results

4.1. Qualitative representation of the plume

The seasonality of surface salinity in the region, characterized by summer spreading and winter retraction (Walker et al., 1996; Morey et al., 2003a; Androulidakis and Kourafalou, 2013) is evident

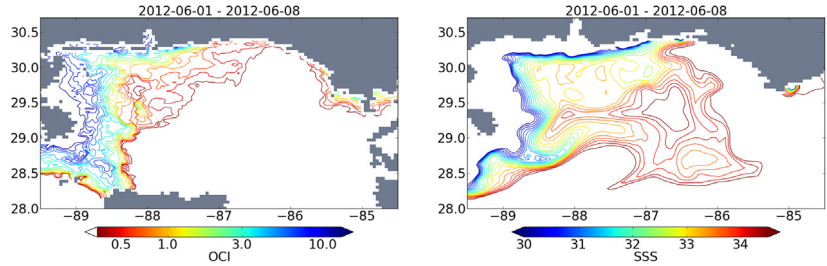

(a) Satellite.

(b) DSC-ROMS.

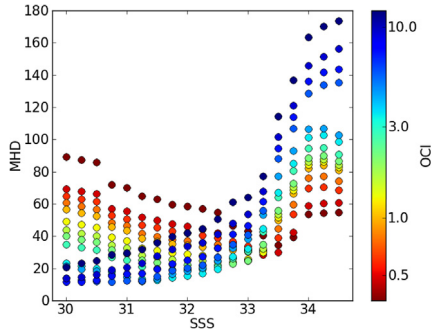

(c) MHD.

Fig. 7. Contours of satellite OCI (a) and SSS from the DSC-ROMS (b) for a particular 8-day average (1–8 June 2012). (c) The corresponding MHD values for each SSS–OCI pair, with SSS on the horizontal axis and OCI value indicated by marker color. (For interpretation of the references to color in this figure legend, the reader is referred to the web version of this article.)

in the satellite OCI and model SSS contours (Figs. 3 and 4). During the fall and winter OCI and SSS contours are often compacted near the coast as northwestward prevailing winds drive a coastally trapped current. During the spring and summer, generally northward winds allow spreading to the east consistent with Ekman drift, where mesoscale circulation features over this deeper region can transport the low salinity water further south (Morey et al., 2003b). Features such as filaments and smaller scale structures and undulations in the contours can be seen in the model SSS and OCI contours at the 4 km resolution, although model fields have increased complexity at their higher native resolutions.

In general, the near shore riverine waters correspond to values of OCI of 5 and above. Further from the Mississippi Delta (the far field), values of OCI less than 0.35 approach the values of the ambient Gulf of Mexico waters making the full extent of the river plume difficult to distinguish. The optical properties of the offshore waters of the Gulf of Mexico have a distinct seasonal cycle largely due to changes in the mixed layer (e.g. Muller-Karger et al., 2015). OCI values between 0.37 and 12.19 are taken to be representative of riverine water in the region and 15 values in this range, selected incrementally on a logarithmic scale, are compared to model SSS contours.

Contours of SSS values from 30 to 34.5 with increments of 0.25 are computed from the re-gridded model data. This range spans waters from the edges of the near field plume to the outer far field where riverine waters have largely mixed with the open ocean waters and approach the ambient salinity of the offshore Gulf of Mexico. The structure of the plume varies between the models (Figs. 3 and 4): GoM-HYCOM, the coarsest native resolution model with climatological river forcing, generally has a broad spread of smoother contours, with little clustering and few small scale variations. NGoM-HYCOM and DSC-ROMS, with increased native resolution and high frequency river forcing, show some additional detail in the contours and smaller scale features such as filaments. DSC-ROMS tends to have more of the lower salinity riverine water pushed further offshore compared to the GoM-HYCOM and NGoM-HYCOM in which the lower salinity riverine water does not generally extend as far offshore.

4.2. Comparison of MHD scores between models

The MHD scores for all OCI–SSS contour pairings are calculated for each model and each eight-day segment for the time period February 2010–February 2013, the longest time common to all datasets. For each of the 285 OCI–SSS pairings per model, the MHD scores are averaged over time resulting in one MHD score per pair per model (Fig. 8(a)–(c)). For a given SSS, the OCI value that yields the minimum MHD score (i.e. best match) can be identified (and vice versa). This provides a set of best pairings that can be compared between models, Fig. 8(d). It should be noted that there is not an exact one-to-one correspondence between the pairings based on minimum MHD distances computed for each SSS contour and for each OCI contour. This is due to the spacing between values of the SSS and OCI contours chosen for this analysis. For example, in one region, several SSS contours may cluster in between more widely spaced OCI contours. The OCI contours will only be closest in shape to one SSS contour but two SSS contours may have the same OCI contour that is closest in shape. As the resolution of the SSS and OCI space increases, this discrepancy in the correspondence will likely decrease. However, using a substantially finer resolution of the SSS and OCI values will increase the computational cost of the analysis given the already large number of combinations tested for each of the three models over the three year period.

For the best pairings, the minimum MHD scores range from 20 to 40 km (Fig. 8(d)). The values show significant differences between each model, particularly for SSS in the range 31–34 (as determined by the 95% confidence intervals shown in Fig. 8(d)). The MHD values are smaller for the GoM-HYCOM and NGoM-HYCOM than DSC-ROMS by approximately 5–15 km. This indicates a better correspondence of GoM-HYCOM and NGoM-HYCOM simulated SSS spatial patterns with the satellite OCI data across a broad range of OCI values. The exception is for very low salinity and high OCI values, where DSC-ROMS has lower MHD scores.

The OCI–SSS value pairs that give the best MHD scores are not the same for each model. Variations among the best OCI–SSS pairings can be used to analyze the differences between riverine water distributions and salinity biases between models.

4.3. SSS and OCI relationships

The optimal pairings, identified by the minimum MHD scores, are compared between models (Fig. 8). For a specified SSS value, a lower OCI value for the model in the best pairings indicates that the SSS contours are generally further offshore when compared to the other models and vice versa. Alternatively, for a specified OCI value, a lower SSS value in the best pair for a model indicates that model has a low SSS bias relative to the other models.

DSC-ROMS has a lower OCI for a given SSS (and lower SSS for a given OCI) when compared to GoM-HYCOM and NGoM-HYCOM. Therefore, DSC-ROMS tends to simulate fresher water further offshore and tends toward a low SSS bias in this region compared to the other models. At the other end of the spectrum, analysis of the NGoM-HYCOM yields the highest OCI for a given SSS, and higher SSS for a given OCI. Therefore, the model tends to have a high SSS bias relative to the other models over this region of freshwater influence. Thus, overall, from DSC-ROMS to GoM-HYCOM to NGoM-HYCOM the salinity bias moves from fresher to more saline.

All model river representations show a transition from high to low SSS as OCI increases. Considering SSS as a function of OCI defined by the best pairings (Fig. 8(a)–(c)), the SSS values change very abruptly over OCI values from 1 to 2 for DSC-ROMS indicating a more rapid variation in SSS, or a more compact salinity front, compared to the other two models (compare the slope of the quadratic fit lines in Fig. 8(a)–(c)). Furthermore, the transition from low to high salinity water begins at a lower OCI (further from the river source) for DSC-ROMS than for GoM-HYCOM and NGoM-HYCOM. GoM-HYCOM displays a broader transition over a wider range of OCI values than NGoM-HYCOM indicating less defined fronts. This is expected given the lower resolution of GoM-HYCOM, its specification of river input from climatology as opposed to daily measured discharge rates and parameterization of rivers using surface salinity relaxation.

Empirical functions describing the relationship between SSS to OCI were derived from the best pairings for each model (Appendix). For each model, a quadratic function is fit to all of the best pairings

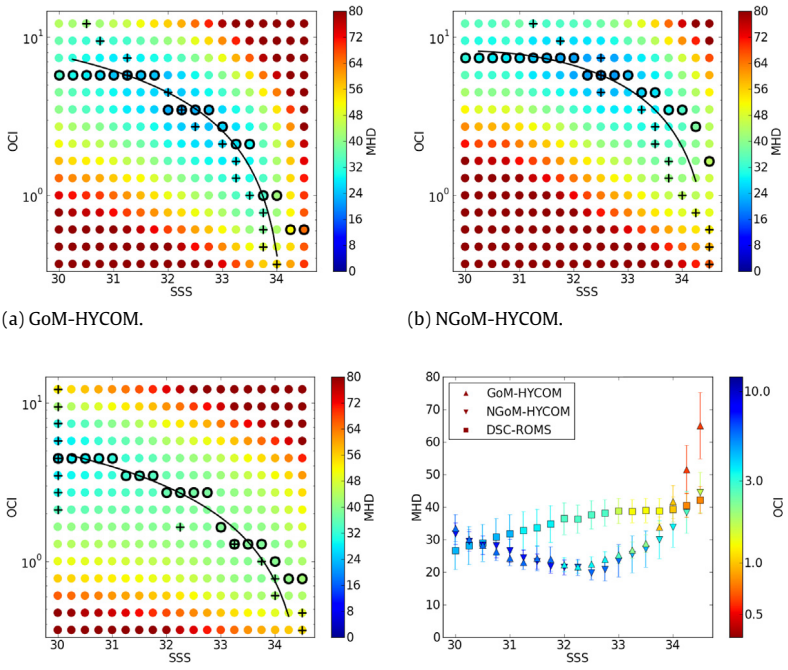

(a) GoM-HYCOM. (b) NGoM-HYCOM.

(c) DSC-ROMS. (d) MHD for best pairings.

Fig. 8. (a)–(c): Time averaged MHD values (indicated by the color of each dot) for each SSS–OCI pairing for each model. Black circles represent the OCI value at which the MHD is minimum for a given SSS and the black crosses represent the SSS value at which the MHD is minimum for a given OCI. These symbols, therefore, represent the best pairings, as determined by the MHD, and can be interpreted for each model as OCI as a function of SSS (black circles), or SSS as a function of OCI (black crosses). The back lines show the monotonic quadratic fit (Appendix) to the best pairings for each model (excluding values at the limits of the ranges of OCI and SSS contours tested). (d): The MHD for each SSS and corresponding best match OCI value. The error bars represent the 95% confidence t-interval (for non-normal data) based on the distribution of MHD values over time for the pairing. (For interpretation of the references to color in this figure legend, the reader is referred to the web version of this article.)

including both those derived from the OCI that yields the minimum MHD for a given SSS and those derived from the SSS that yields the minimum MHD for a given OCI (more details may be found in Appendix). The functions generally indicate a faster rate of change of OCI with SSS at higher SSS values for NGoM-HYCOM and GoM-HYCOM than for the DSC-ROMS simulation (Fig. 8). This may be an indication of generally enhanced lateral mixing in the HYCOM simulations compared to the ROMS simulation.

A picture of the differences in the plumes can be built from the MHD analysis, with DSC-ROMS simulating a large area of low salinity water with a sharp transition to high salinity water and GoM-HYCOM displaying a broader transition from low to high salinity water. NGoM-HYCOM tends towards lower SSS values than GoM-HYCOM, and the riverine water does not spread as far across the domain in NGoM-HYCOM compared to GoM-HYCOM.

5. Discussion and summary

Borrowing from the field of topology, the MHD has been introduced and demonstrated as a tool for quantitative comparison of ocean model fields to satellite remotely sensed data. This approach provides a method to quantify the agreement in shape and spatial structure between fields of either similar or different but related variables as well as producing an empirical relationship between the variables. Typically in ocean modeling, satellite optical data have been used to qualitatively compare features in geophysical fields that are known to manifest changes in the ocean color. By focusing

on shape characteristics, the MHD showcased here provides a numerical metric to complement this qualitative comparison.

The applicability of the MHD has been demonstrated in this work through an analysis of the agreement of the temporal and spatial variability of modeled SSS contours with satellite OCI contours in the vicinity of a large river. A large number of MHD values have been calculated for pairings of multiple SSS and OCI levels at eight-day intervals over a three-year time span, and this information has been condensed into a set of best OCI–SSS pairings for each model. These provide a means to evaluate how well different models simulate the spatial structure and temporal evolution of the salinity field, and to better understand systematic differences (biases) between the models.

Specific differences among the tested models revealed by the MHD analysis include: (1) Lower salinity water is found further offshore in the DSC-ROMS model than in either of the HYCOM models as revealed by the closer matches between lower SSS contour values and the higher OCI contour values that are typically further from the river source. (2) SSS contours for GoM-HYCOM are more broadly spaced than in DSC-ROMS and NGoM-HYCOM as shown by the slower variation of SSS with OCI for the relationship inferred by the set of best pairings. (3) NGoM-HYCOM has the best overall match between the shapes of contours of surface salinity and OCI, followed closely by the GoM-HYCOM and then the DSC-ROMS as shown by the lowest MHD values in the optimum SSS–OCI relationships calculated for each model. These results agree with the visual analysis of the SSS fields and provide a quantitative assessment of the comparison between the models and observations. Furthermore, these findings are in agreement with the ability of NGoM-HYCOM to represent details in the development and evolution of the Mississippi River plume (Androulidakis et al., 2015), as evidenced from comparisons with various other data sources (e.g. Kourafalou and Androulidakis, 2013; Smith et al., 2016).

There are many factors that can affect the simulation of a river plume in models with different numerics and configurations. Important differences between models that impact the dynamics and horizontal spreading of a river plume include among other factors surface forcing (data sources and flux calculations), river parameterization, horizontal and vertical mixing parameterizations, and spatial resolution. For example, the river parameterization in DSC-ROMS prescribes a lateral flux of volume and momentum of fresh water, whereas GoM-HYCOM relaxes the surface salinity in a region surrounding the river source, which is distributed with depth, and NGoM-HYCOM further corrects the pressure to account for the mass influx. The momentum and volume fluxes at the river source may be responsible for the greater offshore penetration of the very low salinity water in DSC-ROMS compared to the two HYCOM simulations. Alternatively, river discharge rates are prescribed differently among the models, which may also account for these differences. The coarser spatial resolution for GoM-HYCOM may lead to more horizontal diffusion and hence weaker salinity gradients inferred from the MHD analysis. A sound investigation of these influences is beyond the scope of this study. However, the MHD offers a diagnostic that would be highly advantageous for such an analysis as it permits objective quantitative skill assessment across models with different river parameterizations and/or within one model for sensitivity testing.

The MHD values for the best contour pairings indicate that GoM-HYCOM and NGoM-HYCOM have a closer match overall in shape of SSS contours with the satellite OCI contours in comparison to the DSC-ROMS model. As GOM-HYCOM is data assimilative, it most likely better represents the mesoscale features that transport low salinity water. NGoM-HYCOM also benefits from the good representation of these features, as it is nested within GoM-HYCOM. Both NGoM-HYCOM and DSC-ROMS are free-running models nested in data-assimilative ocean models. Differences in the nesting procedures, the location of the nesting boundaries and the product the model is nested in may impact how the outer model constrains the mesoscale eddy influences. Significant effort has been placed on parameterization of river inflow in the NGoM-HYCOM, which has been previously assessed with in situ SSS measurements (e.g. Kourafalou and Androulidakis, 2013; Androulidakis and Kourafalou, 2013; Ghani et al., 2014). These are important factors for achieving a better match in shape to the satellite optical observations.

Though the surface salinity in the vicinity of large rivers is linked to structures evident in satellite ocean color imagery, it is important to note that without robust analysis of in situ measurements within the specific region of study one cannot determine which model's agreement to the satellite data is truly "best". In an example of such an exercise, Chaichitehrani et al. (2014) derived CDOM

and SSS relationships from *in situ* observations which were used to calculate CDOM from a numerical model SSS output. The model-derived CDOM was compared to satellite-derived CDOM qualitatively and the model-derived values used to study the factors that affect CDOM distribution. With the MHD, an additional step could be included which would allow quantitative comparison of the satellite-derived CDOM with the model-derived CDOM and determination of an empirical relationship.

Application of the MHD analysis technique to synoptic maps of salinity produced from *in situ* surveys could yield functional relationships between OCI and SSS that could enhance the utility of this procedure to evaluate models. Another benefit of the MHD metric is that it can also be readily used to evaluate model fields with satellite observations of the same variable providing valuable information on the simulated spatio-temporal evolution of the surface fields, even when significant biases exist between the model and satellite observations, as is now commonly the case with simulated biogeochemical fields as well as satellite salinity observations. Furthermore, the MHD provides the comparison between the datasets without the need for visual inspection, allowing automation, as well as quantification. Finally, since the MHD provides a robust metric indicating the agreement between simulated variables and observations, it may be possible to utilize this metric to construct a cost function to be used in an adjoint data assimilation method, allowing assimilation of a wealth of satellite data that are presently underutilized in ocean modeling.

Acknowledgments

This research was made possible by grants from the Bureau of Ocean Energy Management (BOEM) (M12PC00003) and the Gulf of Mexico Research Initiative, and the US NASA (NNX14AM63G and NNX14AL98G). V. Kourafalou acknowledges additional support from NOAA (NA15OAR4320064 and NA15NOS4510226). DSC-ROMS and NGoM-HYCOM model data are publicly available through the Gulf of Mexico Research Initiative Information and Data Cooperative (GRIIDC) at https://data.gulfresearchinitiative.org (UDI: R1.x138.080:0022, UDI: R1.x138.080:0008). The authors would also like to thank Dr. Matthew K. Howard at Texas A&M University for providing river data for the DSC-ROMS simulation and the HYCOM Consortium for providing access to the GoM-HYCOM data at www.hycom.org. The authors would like to thank Dr. Peter Cornillon and one anonymous reviewer for their helpful suggestions.

Appendix. Fitted OCI–SSS functional relationships

For each model, a quadratic function is fit to all of the best pairings including both those derived from the OCI that yields the minimum MHD for a given SSS and those derived from the SSS that yields the minimum MHD for a given OCI (both plus and circle symbols in Fig. 8). Pairings corresponding to the minimum and maximum SSS and OCI values considered in the analysis (boundary rows and columns in Fig. 8(a)–(d)) are excluded to avoid limiting cases impacting the fit. The quadratic functions are constrained to be monotonic over the range of SSS and OCI values tested. The resulting quadratic functions fit to the optimum pairings are:

$$\text{GoM-HYCOM} : OCI = -0.11\,(SSS)^2 + 5.42\,(SSS) - 53.63 \tag{A.1}$$

$$\text{NGoM-HYCOM} : OCI = -0.38\,(SSS)^2 + 23.01\,(SSS) - 337.02 \tag{A.2}$$

$$\text{DSC-ROMS} : OCI = -0.04\,(SSS)^2 + 1.30\,(SSS) - 1.26. \tag{A.3}$$

References

Androulidakis, Y.S., Kourafalou, V.H., 2013. On the processes that influence the transport and fate of Mississippi waters under flooding outflow conditions. Ocean Dyn. 63 (2–3), 143–164.

Androulidakis, Y.S., Kourafalou, V.H., Schiller, R., 2015. Process studies on the Mississippi River plume: impact of topography, wind and discharge conditions. Cont. Shelf Res. 107, 33–49.

Binding, C., Bowers, D., 2003. Measuring the salinity of the Clyde Sea from remotely sensed ocean colour. Estuar. Coast. Shelf Sci. 57, 605–611.

Bleck, R., 2002. An oceanic general circulation model framed in hybrid isopycnic-cartesian coordinates. Ocean Modell. 4, 55–88.
Brekke, C., Solberg, A.H., 2005. Oil spill detection by satellite remote sensing. Remote Sens. Environ. 95, 1–13.
Chaichitehrani, N., D'Sa, E.J., Ko, D.S., Walker, N.D., Osburn, C.L., Chen, R.F., 2014. Colored dissolved organic matter dynamics in the northern Gulf of Mexico from ocean color and numerical model results. J. Coast. Res. 30 (4), 800–814.
Chassignet, E.P., Hurlburt, H.E., Smedstad, O.M., Barron, C.N., Ko, D.S., Rhodes, R.C., et al., 2005. Assessment of data assimilative ocean models in the Gulf of Mexico using ocean color. In: Sturges, W., Lugo-Fernadez, A. (Eds.), AGU Monograph Series, vol. 161. pp. 87–100.
Chassignet, E., Hurlburt, H., Smedstad, O., Halliwell, G., Wallcraft, A., Metzger, E., et al., 2006. Generalized vertical coordinates for eddy-resolving global and coastal ocean forecasts. Oceanography 19 (1), 118–129.
Chassignet, E.P., Smith, L.T., Halliwell, G.R., Bleck, R., 2003. North Atlantic simulations with the Hybrid Coordinate Ocean Model (HYCOM): Impact of the vertical coordinate choice, reference pressure, and thermobaricity. J. Phys. Oceanogr. 2504–2526.
Chonga, Y.J., Khana, A., Scheelbeeka, P., Butlerb, A., Bowersc, D., Vineisa, P., 2014. Climate change and salinity in drinking water as a global problem: using remote-sensing methods to monitor surface water salinity. Int. J. Remote Sens. 35 (4), 1585–1599.
Cummings, J.A., 2005. Operational multivariate ocean data assimilation. Q. J. R. Meteorol. Soc. 131, 3583–3604.
Daoudi, M., Ghorbel, F., Mokadem, A., Avaro, O., Sanson, H., 1999. Shape distances for contour tracking and motion estimation. Pattern Recognit. 32, 1297–1306.
Del Vecchio, R., Subramaniam, A., 2004. Influence of the Amazon River on the surface optical properties of the western tropical North Atlantic Ocean. J. Geophys. Res. Oceans 119, C11. http://dx.doi.org/10.1029/2004JC002503.
Dubuisson, M.-P., Jain, A., 1994. A modified Hausdorff distance for object matching. In: Proceedings of the 12th IAPR International Conference on Pattern Recognition, 1994, pp. 566–568.
Dukhovskoy, D.S., Ubnoske, J., Blanchard-Wrigglesworth, E., Hiester, H.R., Proshutinsky, A., 2015. Skill metrics for evaluation and comparison of sea ice models. J. Geophys. Res. Oceans 120 (9), 5910–5931.
Ghani, M.H., Hole, L.R., Fer, I., Kourafalou, V.H., Wienders, N., Peddie, D., 2014. The SailBuoy remotely-controlled unmanned vessel: measurements of near surface temperature, salinity and oxygen concentration in the Gulf of Mexico. Methods Oceanogr. 10, 104–121.
Green, R.E., Sosik, H.M., 2004. Analysis of apparent optical properties and ocean color models using measurements of seawater constituents in New England continental shelf surface waters. J. Geophys. Res. 109.
Gregg, W.W., 2008. Assimilation of SeaWiFS ocean chlorophyll data into a three-dimensional global ocean model. J. Mar. Syst. 69, 205–225.
Gregg, W.W., Ginoux, P., Schopf, P., Casey, N.W., 2003. Phytoplankton and iron: validation of a global three-dimensional ocean biogeochemical model. Deep Sea Res. Part II 50, 3143–3169.
Hodur, R.M., Pullen, J., Cummings, J., Hong, X., Doyle, J.D., Martin, P., et al., 2002. The Coupled Ocean/Atmosphere Mesoscale Prediction System (COAMPS). Oceanography 15, 88–98.
Hu, C., Barnes, B.B., Qi, L., Corcoran, A.A., 2015. A harmful algal bloom of karenia brevis in the northeastern Gulf of Mexico as revealed by MODIS and VIIRS: A comparison. Sensors 15, 2873–2887.
Hu, C., Lee, Z., Franz, B., 2012. Chlorophyll algorithms for oligotrophic oceans: A novel approach based on three-band reflectance difference. J. Geophys. Res. 117, C01011.
Hu, C., Montgomery, E.T., Schmitt, R.W., Muller-Karger, F.E., 2004. The dispersal of the Amazon and Orinoco River water in the tropical Atlantic and Caribbean Sea: Observation from space and S-PALACE floats. Deep Sea Res. Part II 51, 1151–1171.
Hu, C., Muller-Karger, F.E., Biggs, D.C., Carder, K.L., Nababan, B., Nadeau, D., Vanderbloemen, J., 2003. Comparison of ship and satellite bio-optical measurements on the continental margin of the NE Gulf of Mexico. Int. J. Remote Sens. 24, 2597–2612.
Hu, C., Murch, B., Corcoran, A.A., Zheng, L., Barnes, B.B., Weisberg, R.H., et al., 2016. Developing a smart semantic web with linked data and models for near real-time monitoring of red tides in the eastern Gulf of Mexico. IEEE Syst. J. 99, 1–9.
Huang, R.X., 1993. Real freshwater flux as a natural boundary condition for the salinity balance and thermohaline circulation forced by evaporation and precipitation. J. Phys. Oceanogr. 23 (11), 2428–2446.
Huttenlocher, D., Klanderman, G., Rucklidge, W., 1993. Comparing images using the Hausdorff distance. IEEE Trans. Pattern Anal. Mach. Intell. 15, 850–863.
Huttenlocher, D., Rucklidge, W., 1993. A multi-resolution technique for comparing images using the Hausdorff distance. In: 1993 IEEE Computer Society Conference on Computer Vision and Pattern Recognition, pp. 705–706.
Kourafalou, V.H., Androulidakis, Y.S., 2013. Influence of Mississippi induced circulation on the deepwater Horizon oil spill transport. J. Geophys. Res. 118, 1–20.
Kourafalou, V.H., Peng, H., Kang, H., Hogan, P.J.M.S.O., Weisberg, R.H., 2009. Evaluation of global ocean data assimilation experiment products on South Florida nested simulations with the Hybrid Coordinate Ocean Model. Ocean Dyn. 59 (1), 47–66.
Liu, Y.Y., Weisberg, R.H., Hu, C.C., Kovach, C.C., Riethmuller, R.R., 2013. Evolution of the loop current system during the deepwater horizon oil spill event as observed with drifters and satellites. In: Liu, Y.Y., MacFadyen, A., Ji, Z.-G., Weisberg, R.H. (Eds.), Monitoring and Modeling the Deepwater Horizon Oil Spill: A Record-Breaking Enterprise. American Geophysical Union, pp. 91–101.
Liu, Y., Weisberg, R.H., Hu, C., Zheng, L., 2011. Tracking the deepwater horizon oil spill: A modeling perspective. EOS Trans. Am. Geophys. Union 92, 45–46.
Mariano, A., Kourafalou, V.H., Srinivasan, A., Kang, H., Halliwell, G., Ryan, E., et al., 2011. On the modeling of the 2010 Gulf of Mexico oil spill. Dyn. Atmos. Oceans 52, 322–340.
Mattern, J.P., Fennel, K., Dowd, M., 2010. Introduction and assessment of measures for quantitative model-data comparison using satellite images. Remote Sens. 2, 794–818.
McClain, C.R., 2009. A decade of satellite ocean color observations. Annu. Rev. Mar. Sci. 1, 19–42.
Metzger, E.J., Smedstad, P.G., Thoppil, P.G., Hurlburt, H.E., Cummings, J.A., Wallcraft, A.J., et al., 2014. US Navy operational global ocean and Arctic ice prediction systems. Oceanography 27 (3), 32–43.
Morey, S.L., Martin, P.J., O'Brien, J.J., Wallcraft, A.A., Zavala-Hidalgo, J., 2003a. Export pathways for river discharged fresh water in the northern Gulf of Mexico. J. Geophys. Res. Oceans 108.
Morey, S.L., Schroeder, W.W., O'Brien, J.J., Zavala-Hidalgo, J., 2003b. The annual cycle of riverine influence in the eastern Gulf of Mexico basin. Geophys. Res. Lett. 30.

Morey, S.L., Zavala-Hidalgo, J., O'Brien, J.J., 2005. The seasonal variability of continental shelf circulation in the northern and western Gulf of Mexico from a high-resolution numerical model. In: Sturges, W., Lugo-Fernandez, A. (Eds.), Circulation of the Gulf of Mexico: Observations and Models. In: Geophysical Monograph Series, vol. 161. AGU, Washington, DC, http://dx.doi.org/10.1029/161GM16.
Muller-Karger, F.E., Smith, J.P., Werner, S., Chen, R., Roffer, M., Yanyun Liu, Y., et al., 2015. Natural variability of surface oceanographic conditions in the offshore Gulf of Mexico. Prog. Oceanogr. 134, 54–76.
Nan, Z., Wang, S., Liang, X., Adams, T., Teng, W., Liang, Y., 2010. Analysis of spatial similarities between NEXRAD and NLDAS precipitation data products. IEEE J. Sel. Top. Appl. Earth Obs. Remote Sens. 3, 371–385.
Rosmond, T.E., Teixeira, J., Peng, M., Hogan, T.F., Pauley, R., 2002. Navy Operational Global Atmospheric Predictions System (NOGAPS): Forcing for ocean models. Oceanography 15 (1), 99–108.
Rucklidge, W.J., 1997. Efficiently locating objects using the hausdorff distance. Int. J. Comput. Vis. 24, 251–270.
Saha, S., Moorthi, S., Pan, H.-L., Wu, X., Wang, J., Nadiga, S., et al., 2010. The NCEP climate forecast system reanalysis. Bull. Am. Meteorol. Soc. 91 (8), 1015–1057.
Schiller, R., Kourafalou, V., 2010. Modeling river plume dynamics with the Hybrid Coordinate Ocean Model. Ocean Modell. 33, 101–117.
Schiller, R.V., Kourafalou, V.H., Hogan, P., Walker, N.D., 2011. The dynamics of the Mississippi River plume: Impact of topography, wind and offshore forcing on the fate of plume waters. J. Geophys. Res. Oceans 116 (C6).
Shchepetkin, A.F., McWilliams, J., 2003. A method for computing horizontal pressure-gradient force in an oceanic model with a nonaligned vertical coordinate. J. Geophys. Res. 108 (C3).
Shchepetkin, A.F., McWilliams, J.C., 2005. The Regional Ocean Modeling System: A split-explicit, free-surface, topography following coordinates ocean model. Ocean Modell. 9, 347–404.
Smith, S.R., Briggs, K., Lopez, N., Kourafalou, V.H., 2016. Numerical model evaluation using automated underway ship observations. J. Atmos. Ocean. Technol. 33, 409–428.
Song, Y., Haidvogel, D.B., 1994. A semi-implicit ocean circulation model using a generalized topography-following coordinate system. J. Comput. Phys. 115 (1), 228–244.
Stumpf, R.P., Culver, M.E., Tester, P., Tomlinson, M., Kirkpatrick, G., Pederson, B.A., et al., 2003. Monitoring Karenia brevis blooms in the Gulf of Mexico using satellite ocean color imagery and other data. Harmful Algae 2, 147–160.
Venugopal, V., Basu, S., Foufoula-Georgiou, E., 2005. A new metric for comparing precipitation patterns with an application to ensemble forecasts. J. Geophys. Res.: Atmos. D8, 110.
Walker, N.D., Huh, O.K., Rouse, L.J., Murray, S.P., 1996. Evolution and structure of a coastal squirt off the Mississippi River delta: Northern Gulf of Mexico. J. Geophys. Res. Oceans 101, 20643–20655.
Walker, N.D., Wiseman, W.J., Rouse, L.J., Babin, A., 2005. Effects of river discharge, wind stress, and slope eddies on circulation and the satellite-observed structure of the Mississippi River. J. Coast. Res. 1228–1244.
Zhang, D., Lu, G., 2004. Review of shape representation and description techniques. Pattern Recognit. 37, 1–19.
Zhang, P., Wai, O., Chen, X., Lu, J., Tian, L., 2014. Improving sediment transport prediction by assimilating satellite images in a tidal bay model of Hong Kong. Water 6, 642–660.